Available online at www.sciencedirect.com
ScienceDirect
International Journal of Heat and Mass Transfer 51 (2008) 3753–3762
International Journal of HEAT and MASS TRANSFER
www.elsevier.com/locate/ijhmt

A superposition approach to study slip-flow forced convection in straight microchannels of uniform but arbitrary cross-section

K. Hooman *

School of Engineering, The University of Queensland, Brisbane, Australia

Received 4 October 2007; received in revised form 19 December 2007
Available online 10 March 2008

Abstract

This work presents a superposition approach to investigate forced convection in microducts of arbitrary cross-section, subject to **H1** and **H2** boundary conditions, in the slip-flow regime with further complication of a temperature jump condition assumption. It is shown that applying an average slip velocity and temperature jump definition, one can still use the no-slip/no-jump results with some minor modifications. Present results for slip-flow in microchannels of parallel plate, circular, and rectangular cross-sections are found to be in complete agreement with those in the literature. Application of this methodology to microchannels of triangular cross-section is also verified by comparing the present results with those obtained numerically by undertaking the commercially available software CFD-ACE.

Keywords: Microscale; MEMS; Velocity slip; Temperature jump; Superposition

1. Introduction

Analysis of heat and fluid flow at microscale is of great importance not only for playing a key rule in the biological systems, but also for its application in cooling electronic equipment; see [1–3]. Modeling heat and fluid flow through such small devices is different from the macroscale counterparts in being associated with the inclusion of slip velocity and temperature jump, as noted by Tunc and Bayazitoglu [4]; (see Sparrow and Haji-Sheikh [5] for a pioneering work on velocity slip). For example, a gaseous flow at such small passage does not obey the classical continuum physics where the no-slip condition is valid. Consequently, such a flow is associated with a non-zero fluid velocity at the solid walls and there exists a difference between the gas temperature and that of the wall. This can happen when $0.001 < Kn < 0.1$ while the flow is called slip-flow. For such flow the Navier–Stokes equation should be combined with the slip-flow condition so that the results can match experimental measurements; for more details see [6–10].

Some authors defined a peripherally-averaged slip velocity and temperature jump for forced convection in micorducts of arbitrary cross-sections and solved a new set of equations subject to modified boundary conditions. This paper will show that defining such average slip velocity and temperature jump, one can still use the no-slip and no-temperature jump results, which are available in the literature for both **H1** and **H2** cases (in the terminology of Shah and London [11]).

It should be noted that the temperature field may have different boundary conditions depending on the thermal conductivity of the enclosures. In this study, consideration is given to two different boundary conditions that often appear in the literature being **H1** and **H2**. The former assumes a constant (independent of x^*) longitudinal heat flux while in each cross-section the wall temperature is constant independent of y^* and z^*. The latter, presuming locally constant uniform wall heat flux, allows for the wall temperature to vary with y^* and z^* in each cross-section.

* Tel.: +61 733653585; fax: +61 733654799.
E-mail address: K.Hooman@uq.edu.au

0017-9310/$ - see front matter © 2008 Published by Elsevier Ltd.
doi:10.1016/j.ijheatmasstransfer.2007.12.014

Nomenclature

A	cross-section area, m^2
a	length scale, m
a_{mn}	coefficient defined by Eq. (21c)
B	coefficient defined by Eq. (17)
b	rectangular microduct dimension, m
b^*	aspect ratio for a rectangular microchannel
b_{mn}	coefficient defined by Eq. (23b)
C	microduct inside periphery, m
c_p	specific heat at constant pressure, J/kg K
D_H	hydraulic diameter, m
F	tangential momentum accommodation coefficient
f	friction factor
F_t	thermal accommodation coefficient
k	thermal conductivity, W/m K
Kn	Knudsen number
L_c	characteristic length, m
M_m	eigenvalues, $M_m = (m - 1/2)\pi/b^*$
N_n	eigenvalues, $N_n = (n - 1/2)\pi$
n^*	(coordinate) normal to the wall, m
P^*	pressure, Pa
Po	Poiseuille number
Pr	Prandtl number
r	r^*/R
Re	Reynolds number
s^*	source term, W/m^3
T	absolute temperature, K
u	dimensionless velocity Eq. (6)
u^*	velocity, m/s
U^*	mean velocity, m/s
$\hat{u}$	normalized velocity, u^*/U^*
x^*, y^*, z^*	Cartesian coordinates, m
(x, y, z)	$(x^*, y^*, z^*)/L_c$

Greek symbols

β	slip coefficient
∇^2	dimensionless Laplace operator ($\nabla^2 = L_c^2\tilde{\nabla}^2$)
Γ	tangential coordinate at the microduct wall inside periphery, m
γ	specific heat ratio
λ	molecular mean free path, m
λ_n	eigenvalue, $\lambda_n = (2n - 1)\pi/2$
μ	dynamic viscosity, Pa S
ρ	fluid density, kg/m^3
θ	dimensionless temperature
ψ, φ, Φ	auxillary functions
$\bar{\tau}_w$	average wall shear stress, Pa

Superscript

*	dimensional

Subscripts

m	mean
NS	no-slip
s	fluid properties at the wall
w	wall

Interestingly, the analysis can be extended to porous-saturated microducts subject to slip-flow conditions.

Morini [12] mentioned four technologies to build microchannels. Choosing any of these (or other counterparts) is crucial as the geometry of a micro-flow device strongly depends on the technology used to build it. For example, according to Morini [12], producing microchannels by chemical etching directly on the silicon wafers, the cross-sectional shape depends on a number of factors like the crystallographic nature of the silicon. He also notes that, with other techniques, it is possible to have microchannels of any cross-section. Therefore, more work on convection through microducts of arbitrary cross-sections is called for.

This paper proposes a shorthand way of calculating slip-flow forced convection from the already existing no-slip solutions. Application of this methodology to microchannels of parallel plate, circular, and rectangular ducts is verified by comparing the results with those available in the literature. On the other hand, as there is no result in the literature for a triangular microchannel, applying the commercially available software CFD-ACE, a numerical simulation is also reported for comparison purpose.

2. Problem statement

Consider laminar fully developed forced convection in a straight microconduct of arbitrary but axially uniform

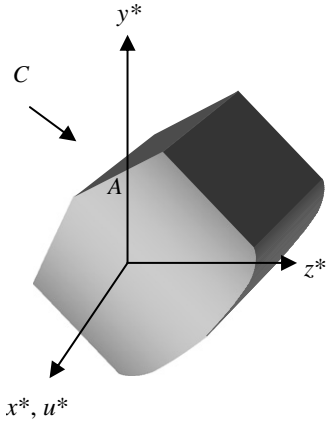

Fig. 1. Schematic diagram of a microchannel of arbitrary but constant shape.

cross-section as shown by Fig. 1. The fluid is assumed to be incompressible with constant properties. This slip velocity can be found as

$$u_s^* = \frac{F-2}{F} Kn D_H \left.\frac{\partial u^*}{\partial n^*}\right|_{wall} \tag{1}$$

where u_s^* is the slip velocity, F is the tangential momentum accommodation coefficient, n^* denotes the coordinate which is normal to the wall, Kn is the Knudsen number ($Kn = \lambda/D_H$), and λ is the molecular mean free path. On the other hand, the fluid temperature at the wall, T_s, can be different form that of the wall, T_w, i.e.

$$T_s - T_w = \frac{F_t - 2}{F_t} D_H \frac{Kn}{Pr} \frac{2\gamma}{1+\gamma} \left.\frac{\partial T*}{\partial n^*}\right|_{wall} \tag{2}$$

Here, F_t is the thermal accommodation coefficient, Pr is the Prandtl number, and γ is the specific heat ratio. The local values of the slip velocity and the temperature jump can change along the duct periphery; however, taking an average over the periphery, these averaged values would be independent of the transverse coordinates. These averages are denoted by an over-bar. For example, with Γ being the tangential coordinate at a point on the microduct wall inside periphery C, the average values (of slip velocity and temperature jump) are

$$\bar{u}_s^* = \int_C u_s^* \, d\Gamma / C$$
$$\overline{T}_s - \overline{T}_w = \frac{F_t - 2}{F_t} \frac{Kn}{Pr} \frac{2\gamma}{1+\gamma} \frac{D_H}{C} \int_C \left.\frac{\partial T*}{\partial n^*}\right|_{wall} d\Gamma \tag{3a, b}$$

where with the **H1** boundary condition $\overline{T}_w = T_w$.

Moreover, similar to Tunc and Bayazitoglu [4], the slip coefficient, β, is obtainable as

$$\beta = \bar{u}_s^* / U^* \tag{4}$$

where $U^* = \langle u^* \rangle$ is the average velocity. The angle brackets denote an average taken over the microconduct cross-section.

The fully developed momentum equation, to be solved subject to slip-flow condition, Eq. (1), is

$$\mu \tilde{\nabla}^2 u^* - \frac{dp^*}{dx^*} = 0 \tag{5}$$

Defining the following dimensionless velocity

$$u = -\mu (u^* - \bar{u}_s^*) / \left(L_c^2 dp^*/dx^*\right) \tag{6}$$

the momentum equation reads

$$\nabla^2 u + 1 = 0 \tag{7}$$

The new set of boundary conditions are $u = 0$ at the walls.

Eq. (7) is the familiar dimensionless form of the fully developed Navier–Stokes equation to be solved subject to no-slip boundary condition, so we replace u by u_{NS}. The function u_{NS} satisfies Eq. (7) subject to no-slip boundary condition (see Shah and London [11] for a variety of solutions for ducts of different cross-sections).

The only unknown is the average slip velocity, $\bar{u}_s^*$, to be found, based on Eqs. (1) and (3a), as follows:

$$\bar{u}_s^* = \frac{F-2}{F} Kn \frac{D_H}{C} \int_C \left.\frac{\partial u^*}{\partial n^*}\right|_{wall} d\Gamma \tag{8}$$

The average wall shear stress, in the fully developed region, is related to the pressure gradient as

$$\bar{\tau}_w = \frac{\mu}{C} \int_C \frac{\partial u^*}{\partial n^*} d\Gamma = -\frac{dp^*}{dx^*} \frac{D_H}{4} \tag{9}$$

Thus $\bar{u}_s^*$ reads

$$\bar{u}_s^* = -\frac{dp^*}{dx^*} \frac{2-F}{F} \frac{Kn}{\mu} D_H \frac{D_H}{4} \tag{10}$$

or in dimensionless form

$$\bar{u}_s = \frac{2-F}{F} Kn \left(\frac{D_H}{2L_c}\right)^2 \tag{11}$$

Eq. (11), in its general form, was also obtainable by applying the Green's function as noted by Haji-Sheikh [13].

Consequently, one finds the velocity distribution for the slip condition as

$$u^* = (-dp^*/dx^*) \left(u_{NS} + \frac{2-F}{F} Kn \left(\frac{D_H}{2L_c}\right)^2 \right) L_c^2/\mu \tag{12}$$

where the average velocity, U^*, reads

$$U^* = (-dp^*/dx^*) L_c^2 \int_A \left(u_{NS} + \frac{2-F}{F} Kn \left(\frac{D_H}{2L_c}\right)^2 \right) dA/(A\mu) \tag{13}$$

Dividing by the velocity scale and dropping the stars, the dimensionless average velocity, U, reads

$$U = U_{NS} + \frac{2-F}{F} Kn \left(\frac{D_H}{2L_c}\right)^2 \tag{14}$$

Note that

$$U_{NS} = \int_A u_{NS} \, dA/A \tag{15}$$

can be obtained from the literature. Then, it is easy enough to define

$$U = \frac{U_{NS}}{B} \tag{16}$$

Combining Eqs. (14) and (16), one gets

$$B = \frac{1}{1 + \frac{2-F}{F U_{NS}} Kn \left(\frac{D_H}{2L_c}\right)^2} \tag{17}$$

One obtains the normalized velocity, $\hat{u} = u^*/U^*$, in terms of no-slip normalized velocity, as

$$\hat{u} = B \hat{u}_{NS} + 1 - B \tag{18}$$

It means that knowing the no-slip results, one can use the above equation to find the normalized velocity distribution in case of a slip-flow. Observe that as $Kn \to 0$ then

$B \to 1$ and the solution tends to that of no-slip, as expected. Note also that Eq. (18) is general as there is no mention of the cross-sectional shape.

It is an easy task to show that the slip coefficient, β, takes the following form:

$$\beta = \frac{Kn}{Kn + \left(\frac{2L_c}{D_H}\right)^2 \frac{FU_{NS}}{2-F}} \tag{19a}$$

or simply

$$\beta = 1 - B \tag{19b}$$

As an example, one can recover the parallel plate microchannel, with $L_c = a$ being the half channel width and $D_H = 4a$, which is the easiest case. For this case, one has $U_{NS} = 1/3$, and $B = \frac{1}{1+(24-12F)Kn/F}$ that leads to $\beta = \frac{(24-12F)Kn/F}{1+(24-12F)Kn/F}$. Moreover, the normalized velocity now takes the following form:

$$\hat{u} = \frac{\frac{3}{2}(1-y^2) + 12\frac{2-F}{F}Kn}{1 + 12\frac{2-F}{F}Kn} \tag{20a}$$

Assuming $F = 1$, one has

$$\hat{u} = \frac{3}{2}\frac{1 + 8Kn - y^2}{1 + 12Kn} \tag{20b}$$

that is in complete agreement with the previous studies; see for example [7,14–16].

As another example, one can mention the case of a microtube, of radius a, where one has U_{NS}=1/8, $B = \frac{1}{1+(16-8F)Kn/F}$, $\beta = \frac{(16-8F)Kn/F}{1+(16-8F)Kn/F}$, and $\hat{u} = \frac{2(1-r^2)+(16-8F)Kn/F}{1+(16-8F)Kn/F}$ which is in line with previous reports, see [15,17] for instance.

For the more complex case of a microduct of rectangular cross-section (size $2a \times 2b$) with aspect ratio $b^* = b/a$, one has $D_H = 4b/(1+b^*)$ where $L_c = a$ leads to

$$B = \frac{1}{1 + \frac{2-F}{FU_{NS}}Kn\left(\frac{2b^*}{1+b^*}\right)^2} \tag{21a}$$

Making use of Eq. (21a) and the average no-slip velocity profile reported by Haji-Sheikh [18], i.e.

$$U_{NS} = \sum_{n=0}^{\infty}\sum_{m=0}^{\infty} a_{mn}$$
$$a_{mn} = \left(\frac{2}{b^* M_m N_n}\right)^2 \frac{1}{M_m^2 + N_n^2} \tag{21b, c}$$

the slip coefficient reads

$$\beta = \frac{Kn}{Kn + \left(\frac{1+b^*}{2b^*}\right)^2 \frac{F}{2-F}\sum_{n=0}^{\infty}\sum_{m=0}^{\infty} a_{mn}} \tag{22}$$

The normalized velocity now takes the following form:

$$\hat{u} = \frac{\sum_{n=0}^{\infty}\sum_{m=0}^{\infty} b_{mn}\cos(M_m z)\cos(N_n y) + \frac{2-F}{F}\left(\frac{2b^*}{1+b^*}\right)^2 Kn}{\sum_{n=0}^{\infty}\sum_{m=0}^{\infty} a_{mn} + \frac{2-F}{F}\left(\frac{2b^*}{1+b^*}\right)^2 Kn}$$
$$b_{mn} = (-1)^{m+n} b^* M_m N_n a_{mn} \tag{23a, b}$$

Besides, the Poiseuille number, $Po = fRe$, which is of particular interest for microchannels, reads

$$Po = \frac{2\bar{\tau}_w}{U^*}\frac{D_H}{\mu} = \frac{2}{U}\left(\frac{D_H}{2L_c}\right)^2 \tag{24a}$$

Note that as $U = U_{NS}/B$ then $Po = BPo_{NS}$ or

$$Po = B\frac{2}{U_{NS}}\left(\frac{D_H}{2L_c}\right)^2 \tag{24b}$$

For a microchannel of parallel plate, circular, and rectangular cross-section, respectively, one has

$$Po = \frac{24}{1 + (24 - 12F)Kn/F}$$
$$Po = \frac{16}{1 + (16 - 8F)Kn/F} \tag{24c – e}$$
$$Po = \frac{1}{\left(\frac{1+b^*}{2b^*}\right)^2 \sum_{n=1}^{\infty}\frac{1}{\lambda_n^4}\left(1 - \frac{\tanh\lambda_n b^*}{\lambda_n b^*}\right) + \frac{2-F}{2F}Kn}$$

It should be noted that Po_{NS} for the rectangular case is taken from Hooman and Merrikh [19] with $\lambda_n = (2n-1)\pi/2$. It is also interesting that Hadjiconstantinou and Simek [20] and Morini et al. [6] have reported a similar Po function for microchannels of parallel plate cross-section. However, absent in their reports was similar correlation for rectangular cross-sections. On the other hand, recent work of Duan and Muzychka [21] lead to a more complicated form of Po while the results are found to be very close to those of present study. Applying the above closed-form solutions, Table 1 is presented to show Po and β, with $F = 1$, for different cross-sections and Kn values.

2.1. Heat transfer aspects: the *H1* case

Assuming constant fluid properties, the fully developed thermal energy equation reads

$$\rho c_p u^* \frac{\partial T^*}{\partial x^*} = k\tilde{\nabla}^2 T^* \tag{25}$$

where, following the application of the first law of thermodynamics to an element, the longitudinal temperature gradient takes this form

$$\frac{\partial T^*}{\partial x^*} = \frac{4q''}{\rho c_p U^* D_H} \tag{26}$$

with $D_H = 4A/C$ being the hydraulic diameter.

Making use of Eqs. (26) and (18), the fully developed thermal energy equation can be rewritten as

Table 1
Poiseuille number and the slip coefficient for microchannels of different cross-sections (values in the parenthesis are correspondent to slip coefficient)

Cross-section	*Kn*			
	0	0.001	0.01	0.1
Equilateral triangular	13.3 (0)	13.2119 (0.0066)	12.4688 (0.0625)	7.98 (0.4)
Circle	16 (0)	15.873 (0.0079)	14.8148 (0.0741)	8.8889 (0.4444)
Square	14.2 (0)	14.0916 (0.0076)	13.1857 (0.0714)	8.0261(0.4348)
Rectangle $b^* = 4$	18.3 (0)	18.1225 (0.0097)	16.6675 (0.0892)	9.245 (0.4948)
Parallel plate	24 (0)	23.7154 (0.0119)	21.4286 (0.1071)	10.9091 (0.5454)

$$k\tilde{\nabla}^2 T* = \frac{4L_c^2 q''}{D_H}(B\hat{u}_{NS} + 1 - B) \tag{27}$$

that should be solved subject to $T^* = \overline{T}_s$ on the walls.

Defining $\theta = \frac{T^* - \overline{T}_s}{4q''L_c^2 B/(kD_H)}$, the boundary conditions become $\theta = 0$ at the walls, and the dimensionless thermal energy equation reads

$$\nabla^2\theta = \hat{u}_{NS} + B^{-1} - 1 \tag{28}$$

Generally, it is an easy equation to solve where the source term, the second term in the right-side, is not changing within the duct cross-section.

An easier way of tackling this problem, is to design a decomposition as

$$\theta = \psi + (B^{-1} - 1)\varphi \tag{29}$$

leading to

$$\begin{aligned} \hat{u}_{NS} &= \nabla^2\psi \\ 1 &= \nabla^2\varphi \end{aligned} \tag{30a, b}$$

with $\psi = \varphi = 0$ at the walls. Solution to Eq. (30a) is available in the literature for the most industrially-important ducts, see Shah and London [11] for example. It should be noted that though, in most cases of interest, Eq. (30b) is very simple to solve, the literature on heat conduction can provide us with analytical solutions for it, see Beck et al. [22]. It is also worth commenting that Eq. (7) is similar to Eq. (30b) in being extensively analyzed for different solid bodies subject to isothermal boundary conditions with a uniform internal heat generation.

Once Eqs. (30a and b) are solved, one can apply the solution obtained for θ, to find T^* as

$$T^* = \overline{T}_s + \frac{4q''L_c^2 B}{kD_H}\theta \tag{31}$$

The only unknown is $\overline{T}_s$ that can be found, based on Eq. (3b), as follows:

$$\begin{aligned} \overline{T}_s &= \overline{T}_w + \frac{F_t - 2}{F_t}\frac{Kn}{Pr}\frac{2\gamma}{1+\gamma}\frac{D_H q''}{k}q^* \\ q^* &= \frac{k}{q''C}\int_C \left.\frac{\partial T^*}{\partial n^*}\right|_{wall} d\Gamma \end{aligned} \tag{32a, b}$$

Furthermore, the bulk-wall temperature difference is obtainable as

$$T_b - T_w = \frac{D_H q''}{k}\left(B\theta_b\left(\frac{2L_c}{D_H}\right)^2 - \frac{2 - F_t}{F_t}\frac{2\gamma}{1+\gamma}\frac{Kn}{Pr}q^*\right) \tag{33}$$

with $T_b = \langle \hat{u}T^* \rangle$ being the bulk temperature.

The Nusselt number, Nu, which is normally defined as

$$Nu = \frac{q''D_H}{k(\overline{T}_w - T_b)} \tag{34}$$

takes the following form:

$$Nu = \frac{1}{\frac{2-F_t}{F_t}\frac{2\gamma}{1+\gamma}\frac{Kn}{Pr}q^* - B\theta_b\left(\frac{2L_c}{D_H}\right)^2} \tag{35}$$

For parallel plate microchannel, one has $\psi = (6y^2 - y^4 - 5)/8$ and $\varphi = (y^2 - 1)/2$ leading to

$$-\theta_b = \frac{17 + 168Kn + (24 - 12F)Kn(14 + 140Kn)/F}{35(1 + 12Kn)} \tag{36}$$

With $L_c = a$, $D_H = 4a$, and $q^* = 1$, Nu reads

$$Nu = \frac{1}{\frac{2-F_t}{F_t}\frac{2\gamma}{1+\gamma}\frac{Kn}{Pr} + \frac{17F + 168KnF + (24-12F)Kn(14+140Kn)}{140(1+12Kn)(F+(24-12F)Kn)}} \tag{37}$$

Assuming air as the fluid, with $\gamma = 1.4$ and $F = F_t = 1$, $Pr = 0.7$, one has

$$Nu = \frac{420(1 + 12Kn)^2}{51 + 28Kn(3600Kn^2 + 780Kn + 61)} \tag{38}$$

Considering a microtube as another example, one has $q^* = 1$, $\psi = (4r^2 - r^4 - 3)/8$, and $\varphi = (r^2 - 1)/4$ leading to

$$-\theta_b = \frac{11 + 64Kn + (16 - 8F)8Kn(1 + 6Kn)/F}{48(1 + 8Kn)} \tag{39}$$

with $L_c = a$ and $D_H = 2a$, the Nusselt number reads

$$Nu = \frac{1}{\frac{2-F_t}{F_t}\frac{2\gamma}{1+\gamma}\frac{Kn}{Pr} + \frac{11+64Kn+(16-8F)8Kn(1+6Kn)/F}{48(1+8Kn)(1+(16-8F)Kn/F)}} \tag{40}$$

Similar to the previous example, one assumes $F = F_t = 1$, $Pr = 0.7$, and $\gamma = 1.4$ to observe that

$$Nu = \frac{144(1 + 8Kn)^2}{33 + 48Kn(320Kn^2 + 104Kn + 13)} \tag{41}$$

Following Haji-Sheikh [18], for a duct of rectangular cross-section the no-slip/no-jump temperature distribution is obtainable as

$$\psi = -\frac{1}{U_{NS}} \sum_{n=0}^{\infty} \sum_{m=0}^{\infty} \frac{b_{mn}}{M_m^2 + N_n^2} \cos(N_n y) \cos(M_m z) \tag{42}$$

Besides, one can obtain φ as follows

$$\varphi = -\sum_{n=0}^{\infty} \sum_{m=0}^{\infty} b_{mn} \cos(N_n y) \cos(M_m z) \tag{43}$$

Combining Eqs. (42 and 43) with Eq. (21a), one has

$$\theta = \sum_{n=0}^{\infty} \sum_{m=0}^{\infty} G_{mn} \cos(N_n y) \cos(M_m z) \tag{44a}$$

wherein

$$G_{mn} = \frac{b_{mn}}{U_{NS}} \left(\frac{F-2}{F} Kn \left(\frac{2b^*}{1+b^*} \right)^2 - \frac{1}{M_m^2 + N_n^2} \right) \tag{44b}$$

The bulk temperature now reads

$$\theta_b = \frac{1}{4U_{NS}} \sum_{n=0}^{\infty} \sum_{m=0}^{\infty} b_{mn} G_{mn} \tag{45}$$

Finally, having θ_b from the above equation, Nu is readily obtainable as

$$Nu = \frac{-1}{B\theta_b \left(\frac{1+b^*}{2b^*}\right)^2 - \frac{2-F_t}{F_t} \frac{2\gamma}{1+\gamma} \frac{Kn}{Pr} q^*} \tag{46-a}$$

with

$$q^* = \frac{-B}{b^*} \sum_{n=0}^{\infty} \sum_{m=0}^{\infty} G_{mn} (-1)^{m+n} \left(\frac{M_m}{N_n} + \frac{N_n}{M_m} \right) \tag{46-b}$$

The analysis can be extended to other cases (asymmetric heating) of the **H1** boundary condition, like those reported by Kuddusi [23], where the no-slip/no-jump solutions can be found in Hooman et al. [24].

2.2. Heat transfer aspects: the H2 case

For this case, the analysis is similar to the **H1** case with the only difference that the boundary conditions for the temperature are of the second kind, i.e.

$$q'' = -k \left. \frac{\partial T^*}{\partial n^*} \right|_{wall} \tag{47}$$

This means that $q^* = 1$ so that the temperature jump reads

$$\overline{T}_s - T_w = \frac{q'' D_H}{k} \frac{2 - F_t}{F_t} \frac{Kn}{Pr} \frac{2\gamma}{1+\gamma} \tag{48}$$

The thermal energy equation, Eq. (27), is still valid while there is a need to (at least) two filtering functions to homogenize the boundary conditions for T, which is the transformed temperature profile. Doing this, another source term, say a function like, s^* will emerge in the thermal energy equation as follows

$$k\tilde{\nabla}^2 T + s^* = \frac{4L_c^2 q''}{D_H} (B\hat{u}_{NS} + 1 - B) \tag{49}$$

Next task is to solve Eq. (49) subject to $\frac{\partial T}{\partial n^*}|_{wall} = 0$. Available in the literature is a great deal of information on solving similar problems, as reviewed by Shah and London [11]. Consequently, one has the solution for T and, in a similar fashion, T^* will be obtained. Finally, one integrates T^* over the duct periphery to find the average wall temperature, to apply in Eqs. (3b) and (34), that, along with the average wall temperature, leads to the Nusselt number. As an example, by recovering the analytical solution reported by Hooman and Haji-Sheikh [25], we show the procedure for a duct of rectangular cross-section ($2b \times 2a$) of aspect ratio $b^* = b/a$. They defined the transformed dimensionless temperature as

$$\Phi = \frac{T - T_i}{q''a/k} = \frac{T^* - T_i}{q''a/k} - \left(\frac{y^2}{2} + \frac{z^2}{2b^*} \right) \tag{50}$$

leading to $s = (1 + b^*)/b^*$, i.e.

$$\frac{4a}{D_H} (B\hat{u}_{NS} + B - 1) = \nabla^2 \Phi + 1 + b^{*-1} \tag{51}$$

Eq. (51), in its turn, can be decomposed into two easier equations as

$$\Phi = C_1 \Phi_1 + C_2 \Phi_2 \tag{52}$$

wherein

$$\nabla^2 \Phi_1 = \hat{u}_{NS} (4a/D_H) \qquad \nabla^2 \Phi_2 = 1 \tag{53a, b}$$

The wall boundary conditions, for $i = 1, 2$, are

$$\partial \Phi_i / \partial n = 0 \tag{54}$$

while the coefficients C_i are

$$C_1 = B, \qquad C_2 = \frac{4a}{D_H} (B - 1) - (1 + b^{*-1}). \tag{55a, b}$$

Solution to Eqs. (55a and b) are available in Haji-Sheikh [18] Haji-Sheikh et al. [26], and Yu and Ameel [27] so that, the local and average wall temperature functions are readily obtainable and, consequently, the bulk temperature can be determined. Finally, the Nusselt number reads

$$Nu = \frac{D_H/a}{C_1[\Phi_{w,1} - < \hat{u}\Phi_1 >] + C_2[\Phi_{w,2} - < \hat{u}\Phi_2 >]} \tag{56}$$

The remaining steps are very similar to those for the examples given for the **H1** case and, mainly for this reason, are not repeated here.

3. Microchannels of triangular cross-sections

3.1. Theoretical analysis

Emphasizing on the generality of the proposed method, based on the findings of previous sections, this section, presents the velocity and temperature distribution in a microduct of triangular cross-section, subject to slip velocity and

temperature jump condition. It is worth noting that there is no closed-form solution for microducts of triangular cross-section, to the best of the author's knowledge, while (extensive) numerical calculations can be an alternative approach as reported by Zhu and Liao [28,29]. Another way of tackling the problem is to use the approximate solutions reported by Bahrami et al. [30] for no-slip case. However, as it will be shown later, application of no-slip results for flow of a rarefied gas can lead to erroneous results. Throughout this work what meant by the triangular cross-section is an equilateral triangle. However, it should be noted that the method is equally applicable to other triangular cross-sections.

Considering an equilateral triangular microduct of side $2a\sqrt{3}$, with $L_c = a$, formed by the region restricted by $z^* = a, z^* + 2a = y^*\sqrt{3}$, and $z^* + 2a = -y^*\sqrt{3}$, the no-slip velocity profile, as reported by Tyagi [31], is

$$u_{NS} = \frac{(1-z)((z+2)^2 - 3y^2)}{12} \tag{57}$$

with

$$U_{NS} = \frac{3}{20} \tag{58}$$

By definition, the coefficient B is obtainable as

$$B = \frac{1}{1 + \frac{40-20F}{3F}Kn} \tag{59}$$

Based on Eq. (18) the normalized velocity should be

$$\hat{u} = \frac{5}{3}\frac{(1-z)((z+2)^2 - 3y^2) + 12(2-F)Kn/F}{3 + (40-20F)Kn/F} \tag{60}$$

One also obtains the average velocity and the slip coefficient as

$$U = \frac{3}{20}\left(1 + \frac{40-20F}{3F}Kn\right) \tag{61}$$

and

$$\beta = \frac{1}{1 + \frac{3F}{40-20F}\frac{1}{Kn}} \tag{62}$$

The temperature distribution is now obtainable as we have

$$\psi = \frac{-5(z-1)((z+2)^2 - 3y^2)(y^2 + z^2 - 4)}{162} \tag{63}$$

and

$$\varphi = \frac{(z-1)((z+2)^2 - 3y^2)}{12} \tag{64}$$

that will result in

$$\theta = \frac{5(z-1)}{162}((z+2)^2 - 3y^2)\left(18\frac{2-F}{F}Kn + 4 - y^2 - z^2\right) \tag{65}$$

The bulk temperature

$$-\theta_b = \frac{9}{28}\left(1 + 80Kn\frac{2-F}{9F}\left(1 + 7\frac{2-F}{3F}Kn\right)\right)\frac{1}{1 + \frac{40-20F}{3F}Kn} \tag{66}$$

will lead to the following Nusselt number:

$$Nu = \frac{\left(1 + \frac{40-20F}{3F}Kn\right)^2}{\frac{2-F_t}{F_t}\frac{8\gamma}{1+\gamma}\frac{Kn}{9Pr}\left(2 + 15\frac{2-F}{F}Kn\right)\left(1 + \frac{40-20F}{3F}Kn\right) + \frac{9}{28}\left(1 + 80Kn\frac{2-F}{9F}\left(1 + 7\frac{2-F}{3F}Kn\right)\right)} \tag{67}$$

Assuming $F = F_t = 1$ and $\gamma = 1.4$, Nu reads

$$Nu = \frac{28}{9}\frac{\left(1 + \frac{20Kn}{3}\right)^2}{1 + \frac{80}{27}Kn\left(\frac{49}{270Pr}(2 + 15Kn)(3 + 20Kn) + 3 + 7Kn\right)} \tag{68}$$

3.2. Numerical details

Commercially available software CFD-ACE (ESI Software) is used, similar to Famouri and Hooman [32], to solve the full set of momentum and thermal energy equation subject to slip-flow condition. Numerical values of

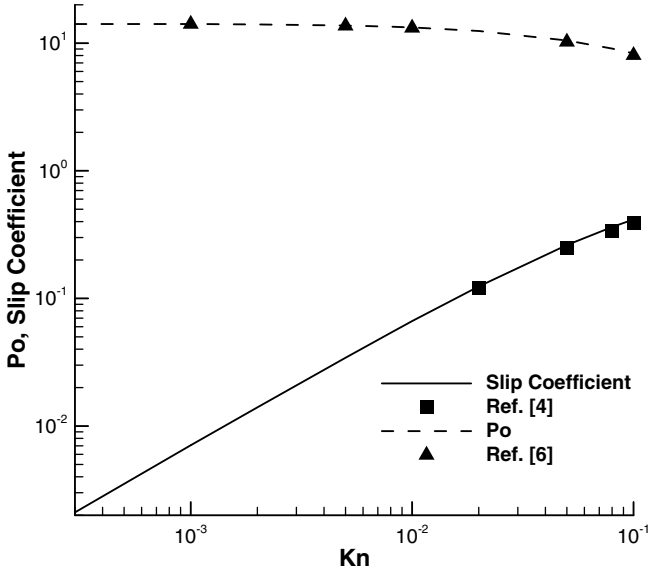

Fig. 2. β and fRe versus Kn compared with previous studies for a microchannel of rectangular cross-section.

the key parameters are selected to be identical to those mentioned in the previous sections, for example $F = 1$, $Pr = 0.7$, and $\gamma = 1.4$. While the inlet velocity, temperature and pressure are assumed to be known, a constant and uniform heat flux at the walls along with Eq. (26) (showing the global energy balance), gives the outlet bulk temperature. The computational domain, a triangular microduct of dimensionless side 3.46 and length 50, was generated with triangular grids for this 3D geometry using the commercial package CFD-GEOM (ESI Software) that is typically used in conjunction with the commercially available finite volume flow solver CFD-ACE.

Grids were controlled in CFD-GEOM using curvature criterion, transition factor, and maximum and minimum cell sizes. For each cross-section these values were 30°, 1.1, 0.25, and 0.00003, respectively. The results were found to be accurate when 15 points on each side of the triangular cross-section (a total of 45 on the periphery) and 100 points

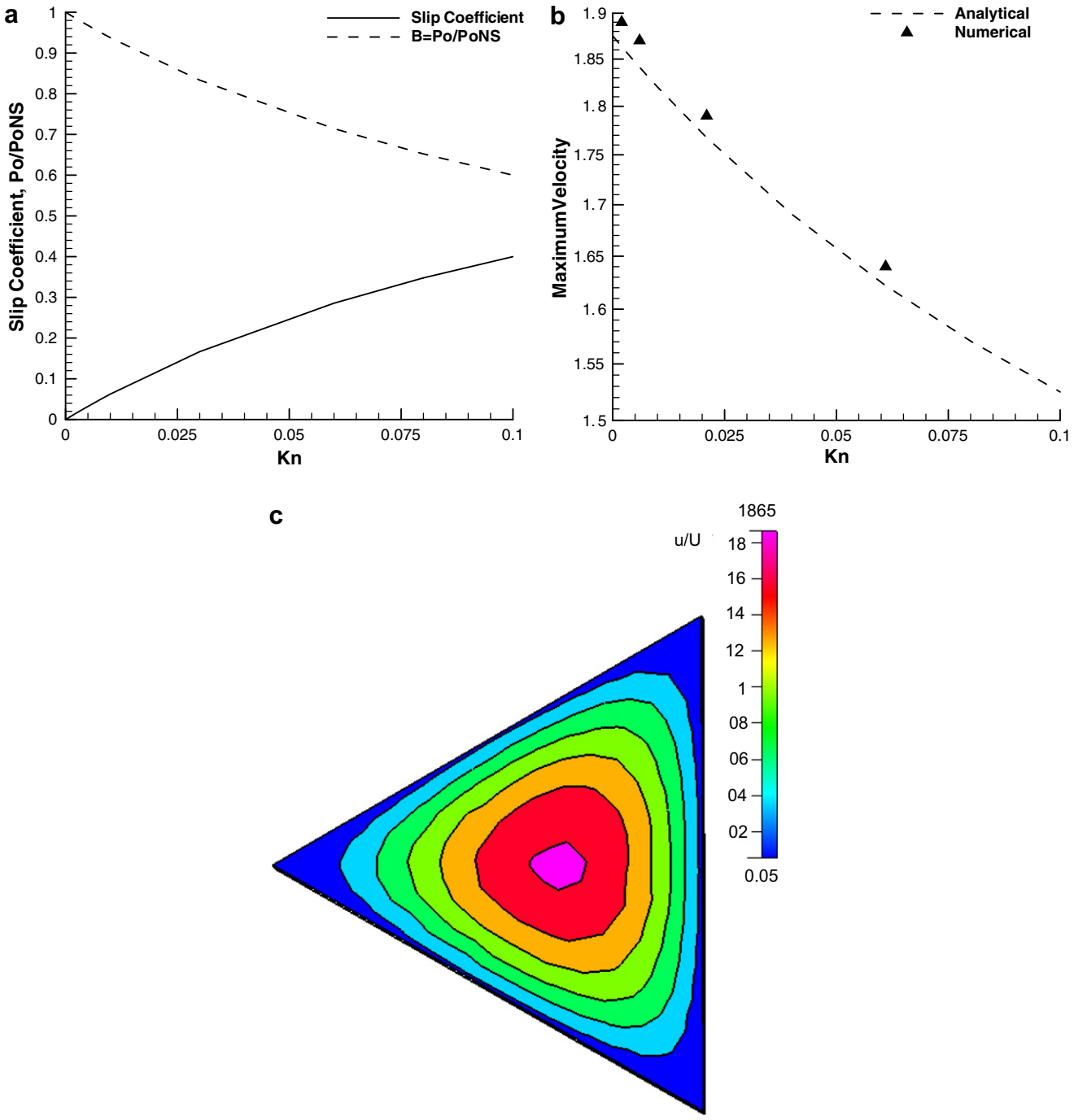

Fig. 3. (a) Slip coefficient and Po/Po_{NS}, (b) maximum normalized velocity versus the Knudsen number, and (c) contours of normalized velocity ($Kn = 0.004$) for a microduct of triangular cross-section ($F = 1$).

in longitudinal direction were applied. This combination has lead to 20,790 cells. Grid-independence was tested by control runs on a finer grid with 41,580 cells that produced consistent results (with a maximum error being less than 3%). Hence, finer grids were not used in reporting the results. It should be noted that the convergence criterion (maximum relative error in the values of the dependent variables between two successive iterations) in all runs was set at 10^{-5}.

4. Discussion

Closed-form solutions for parallel plate and circular microchannels were validated in previous sections. On the other hand, as the obtained results for rectangular microducts were originated from no-slip results there is no need for further check versus macroducts. However, to show the accuracy of the results for slip-flow cases, Fig. 2 is presented to compare present closed-form solutions with those of previously published articles. According to this figure, present results are in good agreement with those in the literature.

Table 1 indicates the Poiseuille number and the slip coefficient for the cases studied here. As Po_{NS} is independent of*Kn,* one concludes that the effect of rarefaction is to cause a decline in *Po*. According to this table, the reduction in *Po* can figure out at 44%, 44%, 50%, and 55% for circular, square, rectangular ($b^* = 4$), and parallel plate cases, respectively. This is in line with previous results of Morini et al. [6], Zhu et al. [28], Renksizbulut et al. [7], and Chen [33]. At the same time, increasing *Kn* will lead to higher β values, as expected. Note that for the case of a parallel plate microchannel β can put on as high values as 0.54 when $Kn = 0.1$. This means that slip velocity can be as high as $0.54U^*$.

Fig. 3a is presented to show the slip coefficient and the Poiseuille number divided by those of no-slip counterparts for a triangular microduct. As seen, increasing *Kn* decreases/increases Po/β. This is expected as increasing *Kn* can be interpreted as higher rarefaction that, in turn, can lead to higher values for the slip velocity and, hence, β should put on higher values. This is inline with the previous studies for microducts of rectangular cross-section; see for example [4] or [34].

Fig. 3b shows the maximum normalized velocity, for flow through a triangular microduct, versus *Kn*. According to this figure, rarefaction can cause a decrease in the maximum velocity hinting that the velocity profile becomes flattened which can lead to higher heat transfer rate. However, this expected enhancement is affected by the presence of the temperature jump similar to what reported by [27,35] for a microchannel of rectangular cross-section. This figure also compares theoretical results with numerical counterparts. As expected, the results are very close and the deviation is less than 2%.

Fully developed velocity contours are depicted in Fig. 3c as another sample of the numerical results. It is interesting to note that the fluid velocity puts on a non-zero value in the near-wall region. More importantly, this slip velocity is uniform along the duct periphery. This gives more credit to the definition of an average slip velocity, $\bar{u}_s^*$. Though both u_s^* and T_s can vary with y^* and z^*, the present approach, that takes an average of these two variables along the duct periphery, leads to reasonably accurate results (at least for the cases studied here).

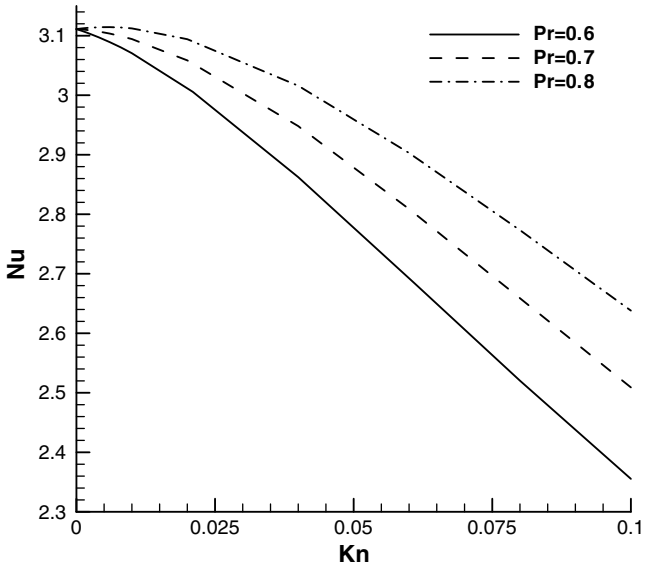

Fig. 4. The Nusselt number versus *Kn* for different values of *Pr* with $\gamma = 1.4$ and $F = F_t = 1$ for a microduct of triangular cross-section subject to **H1** boundary condition.

So far the Prandtl number value was fixed at 0.7 so there is a need to see its effect on the Nusselt number. Fig. 4 shows the Nusselt number versus *Kn* for some values of *Pr*. Seemingly, effect of rarefaction is to reduce *Nu* and this is in line with the findings of Zhu et al. [36] for slip-flow through a triangular microduct subject to cases 2 and 3 of **H1** boundary condition. On the other hand, an increase in *Pr* enhances convection as reflected in higher *Nu* levels. This could also be concluded based on Eq. (67). For $Pr = 0.6$ an increase in *Kn* from 0 to 0.1 causes a 24% decrease in *Nu* while an increase in $Pr = 0.6$–0.8 leads to nearly 14% increase in *Nu* when $Kn = 0.1$.

5. Conclusion

A new approach has been proposed to analyze heat and fluid flow in microchannels of axially uniform but arbitrary cross-section. One does not need to solve the governing equations subject to temperature jump and/or slip velocity boundary condition as the present superposition technique will provide the solver with the solution in terms of those available in the literature for no-jump and/or no-slip cases. A comparison between present results, for slip velocity and temperature jump, with those available in the literature has shown excellent agreement. Fresh theoretical analysis of slip-flow forced convection in microchannels of triangular

cross-sections is also presented to emphasis on the applicability of the proposed approach. However, one should note that application of this method is restricted to laminar steady fully developed (both thermally and hydrodynamically) forced convection flow of an incompressible fluid with constant properties.

Acknowledgements

The financial support provided by The University of Queensland in terms of UQILAS, Endeavor IPRS, and School Scholarship is greatly acknowledged.

References

[1] A.A. Merrikh, J.L. Lage, The role of red cell movement on alveolar gas diffusion, Materialwiss. Werkst. 36 (10) (2005) 497–504.
[2] S.G. Kandlikar, W.J. Grande, Evolution of microchannel flow passages – thermohydraulic performance and fabrication technology, Heat Transfer Eng. 24 (1) (2003) 3–17.
[3] G.L. Morini, Scaling effects for liquid flows in microchannels, Heat Transfer Eng. 27 (4) (2006) 64–73.
[4] G. Tunc, Y. Bayazitoglu, Heat transfer in rectangular microchannels, Int. J. Heat Mass Transfer 45 (4) (2002) 765–773.
[5] E.M. Sparrow, A. Haji-Sheikh, Velocity profile and other local quantities in free-molecule tube flow, Phys. Fluids 7 (8) (1964) 1256–1261.
[6] G.L. Morini, M. Spiga, P. Tartarini, The rarefaction effect on the friction factor of gas flow in microchannels, Superlattice. Microstruct. 35 (3–6) (2004) 587–599.
[7] M. Renksizbulut, H. Niazmand, G. Tercan, Slip-flow and heat transfer in rectangular microchannels with constant wall temperature, Int. J. Therm. Sci. 45 (9) (2006) 870–881.
[8] A.A. Rostami, A.S. Mujumdar, N. Saniei, Flow and heat transfer for gas flowing in microchannels: a review, Heat Mass Transfer 38 (4–5) (2002) 359–367.
[9] M. Gad-El-Hak, Gas and liquid transport at the microscale, Heat Transfer Eng. 27 (4) (2006) 13–29.
[10] M. Gad-el-Hak, Liquids: the holy grail of microfluidic modeling, Phys. Fluids 17 (10) (2005).
[11] R.K. Shah, A.L. London, Laminar Flow Forced Convection in Ducts: A Source Book for Compact Heat Exchanger Analytical Data, Academic Press, New York, 1978.
[12] G.L. Morini, Single-phase convective heat transfer in microchannels: a review of experimental results, Int. J. Therm. Sci. 43 (7) (2004) 631–651.
[13] A. Haji-Sheikh, Private communication, 2007.
[14] H.E. Jeong, J.T. Jeong, Extended Graetz problem including streamwise conduction and viscous dissipation in microchannel, Int. J. Heat Mass Transfer 49 (13–14) (2006) 2151–2157.
[15] K. Hooman, Entropy generation for microscale forced convection: effects of different thermal boundary conditions, velocity slip, temperature jump, viscous dissipation, and duct geometry, Int. Commun. Heat Mass Transfer 34 (8) (2007) 945–957.
[16] N.G. Hadjiconstantinou, Dissipation in small scale gaseous flows, J. Heat Transfer – Trans. ASME 125 (5) (2003) 944–947.
[17] H.E. Jeong, J.T. Jeong, Extended Graetz problem including axial conduction and viscous dissipation in microtube, J. Mech. Sci. Technol. 20 (1) (2006) 158–166.
[18] A. Haji-Sheikh, Fully developed heat transfer to fluid flow in rectangular passages filled with porous materials, J. Heat Transfer – Trans. ASME 128 (6) (2006) 550–556.
[19] K. Hooman, A.A. Merrikh, Analytical solution of forced convection in a duct of rectangular cross section saturated by a porous medium, J. Heat Transfer – Trans. ASME 128 (6) (2006) 596–600.
[20] N.G. Hadjiconstantinou, O. Simek, Constant-wall-temperature Nusselt number in micro and nano-channels, J. Heat Transfer – Trans. ASME 124 (2) (2002) 356–364.
[21] Z.P. Duan, Y.S. Muzychka, Slip flow in non-circular microchannels, Microfluid Nanofluid 3 (4) (2007) 473–484.
[22] J.V. Beck, K. Cole, A. Haji-Sheikh, B. Litkouhi, Heat Conduction Using Green's Functions, Hemisphere Publ. Corp., Washington, DC, 1992.
[23] L. Kuddusi, Prediction of temperature distribution and Nusselt number in rectangular microchannels at wall slip condition for all versions of constant wall temperature, Int. J. Therm. Sci. 46 (2008) 998–1010.
[24] K. Hooman, H. Gurgenci, A.A. Merrikh, Heat transfer and entropy generation optimization of forced convection in a porous-saturated duct of rectangular cross-section, Int. J. Heat Mass Transfer 50 (2007) 2051–2059.
[25] K. Hooman, A. Haji-Sheikh, Analysis of heat transfer and entropy generation for a thermally developing Brinkman–Brinkman forced convection problem in a rectangular duct with isoflux walls, Int. J. Heat Mass Transfer 50 (21–22) (2007) 4180–4194.
[26] A. Haji-Sheikh, D.A. Nield, K. Hooman, Heat transfer in the thermal entrance region for flow through rectangular porous passages, Int, J. Heat Mass Transfer 49 (17–18) (2006) 3004–3015.
[27] S.P. Yu, T.A. Ameel, Slip-flow heat transfer in rectangular microchannels, Int. J. Heat Mass Transfer 44 (22) (2001) 4225–4234.
[28] X. Zhu, Q. Liao, Heat transfer for laminar slip flow in a microchannel of arbitrary cross section with complex thermal boundary conditions, Appl. Therm. Eng. 26 (11–12) (2006) 1246–1256.
[29] X. Zhu, Q. Liao, M.D. Xin, Gas flow in microchannel of arbitrary shape in slip flow regime, Nanoscale Microscale Thermophys. Eng. 10 (1) (2006) 41–54.
[30] M. Bahrami, M.M. Yovanovich, J.R. Culham, Pressure drop of fully-developed laminar flow in microchannels of arbitrary cross-section, J. Fluids Eng. – Trans. ASME 128 (5) (2006) 1036–1044.
[31] V.P. Tyagi, Forced convective heat-transfer including dissipation function and compression work for a class of noncircular ducts, Int. J. Heat Mass Transfer 15 (1) (1972) 164–168.
[32] M. Famouri, K. Hooman, Entropy generation for natural convection by heated partitions in a cavity, Int. Commun. Heat Mass Transfer 35 (4) (2008) 492–502.
[33] C.H. Chen, Slip-flow heat transfer in a microchannel with viscous dissipation, Heat Mass Transfer 42 (9) (2006) 853–860.
[34] K. Hooman, Heat transfer and entropy generation for forced convection through a microduct of rectangular cross-section: effects of velocity slip, temperature jump, and duct geometry, Int. Heat Mass Transfer, submitted for publication.
[35] S.P. Yu, T.A. Ameel, Slip flow convection in isoflux rectangular microchannels, J. Heat Transfer – Trans. ASME 124 (2) (2002) 346–355.
[36] X. Zhu, Q. Liao, M. Xin, Analysis of the heat transfer in unsymmetrically heated triangular microchannels in slip flow regime, Sci. China Ser. E – Eng. Mater. Sci. 47 (4) (2004) 436–446.